ISSN 0016-7932, Geomagnetism and Aeronomy, 2012, Vol. 52, No. 5, pp. 653–663. © Pleiades Publishing, Ltd., 2012.
Original Russian Text © A.A. Cheremisin, P.V. Novikov, I.S. Shnipov, V.V. Bychkov, B.M. Shevtsov, 2012, published in Geomagnetizm i Aeronomiya, 2012, Vol. 52, No. 5, pp. 690–700.

Lidar Observations and Formation Mechanism of the Structure of Stratospheric and Mesospheric Aerosol Layers over Kamchatka

A. A. Cheremisin[a], P. V. Novikov[b], I. S. Shnipov[b], V. V. Bychkov[c], B. M. Shevtsov[c]

[a] *Siberian Federal University, Krasnoyarsk*

[b] *Krasnoyarsk Institute of Rail Transport, Branch of Irkutsk State University of Railway Transport, Krasnoyarsk*

[c] *Institute of Cosmophysical Research and Radiowave Propagation, Far Eastern Branch, Russian Academy of Sciences, ul. Mirnaya 7, Paratunka, Kamchatskaya oblast, 684034 Russia*

e-mail: aacheremisin@gigmail.com, vasily@ikir.kamchatka.ru

Received September 22, 2010; in final form, November 7, 2011

Abstract—Lidar observations during 2007–2008 in Kamchatka revealed aerosol layers in the upper stratosphere at heights of 35–50 km and in the mesosphere at heights of 60–75 km. It is well known that forces of gas–kinetic nature, i.e., photophoretic forces, act on aerosol particles that absorb solar radiation and terrestrial IR radiation; these forces can counteract the gravitational force and even lead to the levitation of these particles at particular heights. The accumulation of particles at these heights may lead to the formation of aerosol layers. We calculated these forces for the conditions of lidar observations in Kamchatka. Aerosol layers were observed at heights where particle levitation can occur. Thus, the stratospheric and mesospheric aerosol layers, detected at heights of 30–50 and 60–75 km, respectively, may be due to the effect of the photophoretic force on aerosol particles.

DOI: 10.1134/S0016793212050027

1. INTRODUCTION

In the last two decades, much progress has been made in studying aerosol particles in the *D* region of the ionosphere, which, if present, can influence significantly the local charge balance and modify the scattering of radiowaves in the ionospheric plasma. Despite the recent great effort directed at studying the mesosphere by means of satellites, rockets, and ground-based sensing facilities, it still remains a poorly studied region of the atmosphere (Friedrich et al., 2009a). Most and, in particular, satellite-based studies (Hervig et al., 2009) are aimed at studying noctilucent (mesospheric) clouds. These clouds are observed at heights of 83–85 km in the Northern Hemisphere and at heights of 84–87 km in the Southern Hemisphere; they comparatively well scatter visible radiation and are actively studied by lidar remote-sensing methods (Fiedler et al., 2009). They can even be observed visually during twilight (Bronshten, 1984). If we exclude noctilucent cloud observations and consider lidar observations of the mesospheric region as a whole, it is conventionally considered that lidar signals reproduce molecular scattering when returned from sensing heights higher than 30 km (Kent and Wright, 1970; Poultney, 1972) and, only in particular cases, such as during large comet impacts, aerosol-scattering layers are observed in the upper stratosphere and mesosphere (Mezheris, 1987). The existence of charged aerosol particles in the mesosphere is inferred by indirect methods from enhanced radiowave scattering at heights of 60–80 (the so-called polar wintertime mesospheric echo) (Zeller et al., 2006) and 80–90 km (the so-called polar summertime mesospheric echo) (Rapp and Lübken, 2004). The presence of charged particles was also indicated by local dips in the electron density, which were observed at a height of 80 km with the help of rocket-based instrumentation in the presence of the summertime mesospheric echo (Friedrich et al., 2009b).

Tangent sensing from space in the UV spectral range indicates that stable aerosol layers exist in the undisturbed upper atmosphere in the equatorial zone and at midlatitudes at heights of ~50, 70, and 93 km (Cheremisin et al., 2000). An aerosol layer at a height of 50 km was first inferred from data of 40-year ground-based twilight observations (Rozenberg et al., 1980). The presence of this layer is qualitatively confirmed by observations of the Earth's twilight horizon from space (Kondratyev et al., 1977; Rozenberg and Sandomirsky, 1971; Giovane et al., 1976; Butov and Loginov, 2001). The presence of the layered structure of the Earth's upper atmosphere is also confirmed by rocket studies (Rossler, 1972; Mikirov and Smerkalov, 1981; Kuznetsov et al., 1977). It was concluded that the known facts regarding aerosol stratification in the middle atmosphere are difficult to interpret in the framework of the existing models, based on the consideration of the processes of sedimentation–diffusion equilibrium with the employment of some or other condensation hypotheses (Cheremisin et al., 2000).

It is well known that forces of gas-kinetic nature, namely, photophoretic forces, can act on aerosol particles that absorb solar and terrestrial IR radiation; these forces can counteract the gravitational force or even lead to the levitation of these particles at certain heights. Particle accumulation at these heights may lead to the formation of aerosol layers (Cheremisin et al., 2005).

Photophoresis is light-induced particle motion. This effect arises in rarefied gases due to the nonuniform accommodation of gas molecules over particle surfaces, e.g., when temperatures or accommodation coefficients vary across particle surfaces. Force fields influence the photophoretic particle motion, and then it is called gravito-photophoresis, magneto-photophoresis, etc. There is abundant experimental evidence of particle levitation in vacuum chambers under the impact of radiation of lasers and other light sources, which is cited in (Cheremisin et al., 2005). The theoretical works (Pueshel et al., 2000; Rohatschek, 1996; Cheremisin et al., 2002; Beresnev et al., 2003; Cheremisin et al., 2005) analyzed the effect of photophoretic forces on the vertical transport of aerosol particles in the atmosphere. It was shown in (Cheremisin et al., 2005) that gravito-photophoretic forces can sustain aerosol layers in the stratosphere and mesosphere at heights of ~20, 50, 70, and 80–83 km in the polar summertime mesosphere, as well as at 30–50 km. The general algorithms for calculating photophoretic forces in complex systems were presented in (Cheremisin, 2010).

Previously, the gravito-photophoretic hypothesis of aerosol stratification was based on comparisons with experimental observation data in general. Cheremisin et al. (2005) analyzed the levitation of aerosol layers under the conditions of the standard atmosphere. An analysis of the seasonal latitudinal pattern of the levitation of layers revealed new features of aerosol stratification under the impact of gravito-photophoresis forces (Cheremisin and Vassilyev, 2006). Hopefully, a more detailed consideration of the geographic and temporal conditions will help to check the gravito-photophoretic hypothesis more accurately. Theoretical calculations can now be compared with experimental observations more thoroughly after the creation of a lidar station in Kamchatka, which can sense within an altitude range from the upper stratosphere to the mesosphere.

The lidar station in Kamchatka (the settlement of Paratunka) has been operational since 2007; it records return signals owing to the elastic scattering of light on air molecules and aerosol particles. Observations of the middle atmosphere began from October 2007. One-year measurements showed that, at heights higher than 40 km, the profile of the lidar signal indicates the presence of aerosol layers in the neighborhood of the stratopause (Bychkov et al., 2008). It should be noted that lidar observations over Tomsk also detected aerosol layers at heights of 35–45 km in the winter time (Bychkov and Marichev, 2008).

This work presents lidar data on aerosol scattering in the upper stratosphere and mesosphere over Kamchatka up to heights of 75–80 km for one-year period from October 2007 to September 2008. The characteristic seasonal features of the occurrence of aerosol layers are identified. We also calculated the heights where aerosol particles can levitate under the impact of gravito-photophoretic forces for those same days and meteorological conditions under which the lidar observations in Kamchatka were performed. The altitude regions of levitation are compared with the heights of the observed aerosol layers.

2. METHOD OF LIDAR OBSERVATIONS OF AEROSOL LAYERS IN THE UPPER STRATOSPHERE AND MESOSPHERE OVER KAMCHATKA

The lidar station at the Institute of Cosmophysical Research and Radiowave Propagation, Far Eastern Branch, Russian Academy of Sciences, Kamchatka, was described in (Bychkov et al., 2008). Here, we will only mention the main characteristics: the radiation is at a wavelength of 532 nm, the energy in the pulse is 0.4 J, the pulse duration is 5 ns, the pulse repetition rate is 10 Hz, the diameter of the receiver mirror is 60 cm, the focal distance is 210 cm, the beam divergence after exit from the collimator is 10^{-5} rad, and the receiver's field of view is 5×10^{-4}–10^{-3} rad. All measurements in this work were performed for a 510-cm distance between the receiver and transmitter axes. The vertical resolution of the measurements is 1.5 km, which is determined by the time resolution of the Hamamatsu-H8784 photon counter of 10 μs; the photomultiplier tube (PMT) is Hamamtsu-M8259-01, and the dark current noise is 20 photons per second at a temperature of 20°C. During the propagation of a laser pulse to heights of ~21 km, we applied electronic gaiting to cut off the signals from the near sensing zone. This reduced the dynamic range of the lidar signal and made it possible to monitor simultaneously the upper stratospheric region and the mesosphere for a relatively moderate aftereffect of the PMT pulses (Vetokhin et al., 1986) on measurements at heights up to 80 km.

The aerosol stratification of the atmosphere was analyzed using the scattering ratio $R(H) = (\beta_{\pi m}(H) + \beta_{\pi a}(H))/\beta_{\pi m}(H)$, where $\beta_{\pi m}(H)$, and $\beta_{\pi a}(H)$ are the molecular and aerosol volume backscattering coefficients at height H. When aerosols are present (absent) at a certain height, $R(H) > 1$ ($R(H) \approx 1$) within the measurement error).

The equation of laser sensing (Samokhvalov et al., 1987) can be written in the following form (Elnikov et al., 1988):

$$R(H) = N_c(H)H^2 \Big/ \left[C\beta_{\pi m}(H)T^2(0,H)\right], \qquad (1)$$

where $N_c(H)$ is the return signal, C is the instrumental constant of the lidar, and $T(0, H)$ is the atmospheric transmission coefficient integrated from the lidar to height H. Constant C is determined using the calibration method of lidar signals from the molecular backscattering coefficient. In this case, it is assumed that aerosol scattering can be neglected at a certain height; then, the equation of laser sensing becomes

$$R(H) = \frac{N_c(H)H^2\beta_{\pi m}(H_0)}{N_c(H_0)H_0^2\beta_{\pi m}(H)T^2(H,H_0)}, \qquad (2)$$

where $N_c(H_0)$, and $\beta_{\pi m}(H_0)$ are the return signal and the molecular scattering coefficient at calibration height H_0 and $T(H,H_0)$ is the transmission coefficient of the atmospheric layer from normalization height H_0 to height H. In the general case, the transmission coefficient $T(H,H_0)$ depends on molecular scattering and the unknown parameters of aerosol scattering and absorption: $T(H,H_0) = \exp(-\tau)$, where $\tau = \int_{H_0}^{H} \alpha(h)dh$ is the optical depth of the atmospheric layer; $\alpha(H) = \beta_m(H) + \beta_a(H) + \gamma_a(H)$ is the total extinction coefficient, where $\beta_m(H)$ is the molecular volume scattering coefficient and $\beta_a(H)$, and $\gamma_a(H)$ are the aerosol volume scattering and absorption coefficients, respectively. Taking into account formula (1), the optical depth can be written as

$$\tau = \int_{H_0}^{H} \left\{\beta_{\pi m}(h)\left[\frac{1}{f_{\pi m}} + \frac{R(h)-1}{f_{\pi a}(h)}\right] + \gamma_a(h)\right\} dh,$$

where $f_{\pi m}$ and $f_{\pi a}$ are the phase functions of molecular and aerosol backscattering, respectively. According to well-known atmospheric models (Atmosfera, 1991; Krekov and Zvenigorodsky, 1990), for an altitude range of 30–80 km, which is studied here, the contribution of aerosol extinction (scattering and absorption) to the optical depth τ on average does not exceed 0.003 and the contribution of molecular scattering is 0.0012. In this regard, we reduced equation (2), by letting $T(H,H_0) = 1$, which leads to the relative error $(\delta R/R)_T \approx 2\delta T/T \approx 2\tau \approx 0.008$. This error makes a minor contribution to the total measurement error. After eliminating the $T(H,H_0)$, transmission from formula (1), its right-hand side can be considered as an expression for calculating $R(H)$ from lidar measurement data for a known altitude dependence of the molecular backscattering coefficient $\beta_{\pi m}(H)$.

3. LIDAR MEASUREMENT ERRORS OF STRATOSPHERC AND MESOSPHERIC AEROSOLS

In addition to the $R(H)$ retrieval error, associated with the accounting for atmospheric transmission in the equation of laser sensing $(\delta R/R)_T^2$, the estimate of which was presented above, we will also consider the contributions of some other known components (Russel et al., 1979; Elnikov et al., 1988) to the total measurement error

$$\left(\frac{\delta R}{R}\right)^2 = \left(\frac{\delta R}{R}\right)_T^2 + \left(\frac{\delta\beta_{\pi m}(H)}{\beta_{\pi m}(H)}\right)^2 + \left(\frac{\delta R}{R}\right)_{\text{к}}^2 + \left(\frac{\delta N_c(H)}{N_c(H)}\right)^2,$$

where $\delta\beta_{\pi m}(H)/\beta_{\pi m}(H)$ is the estimation error of molecular scattering; $(\delta R/R)_{\text{к}}$ is the calibration error; and $\delta N_c(H)/N_c(H)$ is the error of determining the return signal.

The molecular scattering coefficient, defined to be proportional to the number of molecules per unit volume, was calculated according to the Aura satellite data on temperature T and pressure p (Dobber et al., 2006). The Aura satellite data on the errors of the temperature δT and geopotential height δh measurements for fixed pressure levels make it possible to calculate the corresponding contribution to the error $\delta\beta_{\pi m}(H)/\beta_{\pi m}(H) = \sqrt{(\delta p/p)^2 + (\delta T/T)^2}$, where $\delta p/p = \delta h/h_0$, $h_0 = mg/(kT)$ is the height of the homogeneous atmosphere for height h; m is the mean mass of the air molecule; g is the acceleration of gravity; and k is the Boltzmann constant. This relative error varies from 0.006 to 0.016 in an altitude range from 30 to 80 km.

In accordance with equations (1) and (2), the contributions to the error which are associated with the calibration of lidar signals at height H_0 are written as

$$(\delta R/R)_{\text{к}} = \sqrt{(\delta N(H_0)/N(H_0))^2 + (\delta\beta_{\pi m}(H_0)/\beta_{\pi m}(H_0))^2 + (R(H_0)-1)^2},$$

where $N(H_0)$ is the total signal recorded by PMT when $H = H_0$ and $\delta N(H_0) = \sqrt{N(H_0)}$ is the error of the photon counting by PMT, which is estimated on the basis of Poisson statistics of photon counting. The calibration was mainly performed at heights of about 30 km, with the errors $\delta N(H_0)/N(H_0)$ and $\delta\beta_{\pi m}(H_0)/\beta_{\pi m}(H_0)$ being about 0.005 and 0.006, respectively. The main contribution to the calibration error was caused by the assumption that no aerosol was present at calibration height H_0. If the actual value of the scattering ratio is equal to $R(H_0)$, then there appears a contribution to the relative error which is

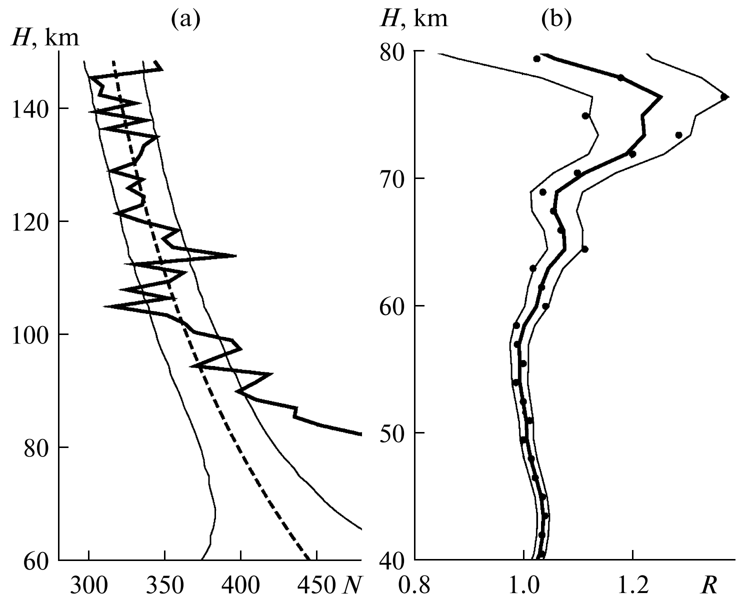

Fig. 1. Lidar observations of aerosol scattering in the atmosphere over Kamchatka on October 28, 2007. (a) Signal corrected for the PMT aftereffect pulses and for the effect of background illumination: the broken line shows the initial PMT signal, the dashed line shows the approximation of the signal above 100 km, and the thin lines show the approximation error corridor. (b) The backscattering ratio after the subtraction of the aftereffect (circles) and subsequent smoothing using the Gaussian filter (thick line); the thin lines indicate the error corridor.

equal to $(R(H_0 - 1)$.The calibration uncertainty leads to the underestimation of the aerosol scattering level within the entire altitude range, i.e., the $R(H)$ curve is shifted relative to the true dependence by the amount $R(H)(\delta R)_{\text{к}}$.

Return signals decay with increasing altitude, and, for the altitude region of the upper stratosphere and, especially, mesosphere, it is necessary to take into account the fact that the total signal $N(H)$, recorded by PMT, includes a few components: $N(H) = N_{\text{signal}}(H) + N_{\text{after}}(H) + N_{\text{back-dark}}$, where $N_{\text{signal}}(H)$ is the sought return signal associated with the scattering of laser radiation in the atmosphere; $N_{\text{after}}(H)$ is the number of the PMT aftereffect pulses (Vetokhin et al., 1986); and $N_{\text{back-dark}}$ is the sum of signals due to background sky illumination (Moon, stars, and other sources) and the intrinsic dark-current PMT noise. The determination error of return signals $\delta N_{\text{signal}}(H) = \sqrt{N(H) + \sigma^2_{\text{approx}}}$ includes the error of photon counting by PMT $\sqrt{N(H)}$, which is estimated on the basis of Poisson statistics of photon counting, and the approximation uncertainty σ_{approx} of the average values $N_{\text{after}}(H) + N_{\text{back-dark}}$.

The two latter quantities were estimated as follows. In our case, at heights of 100–150 km, the return signal turned out to be negligibly small compared to the total signal $N(H)$. At these heights, we approximated $N_{\text{after}}(H) + N_{\text{back-dark}}$ by the dependence $f(H) = a\exp(-bH) + d$, where a, b, and d are constants (Bychkov et al., 2011). This dependence was plotted on the basis of the least squares method (LSM) by minimizing the squared deviations of the experimental points from the approximating curve according to these three parameters for the above-indicated altitude interval and then extrapolated into a lower -altitude region. The d value, resulting from the curve fitting, usually almost coincided with the average background signal $N_{\text{back-dark}}$, according to measurements in the time interval between 20 and 24 ms after sending each light pulse of the laser, i.e., at sensing times corresponding to the heights of the order of 6000 km.

Figure 1a shows the PMT signal $N(H)$ (thick line), the $f(H)$ approximation, and the error corridor of the approximation $\pm\sigma_{\text{approx}}$ for lidar measurements performed in Kamchatka on October 28, 2007, with the signal being accumulated for 1 h and 45 min. As the $f(H)$ approximation itself, the approximation error was obtained using the LSM according to well-known formulas for statistical estimation with linear LSM (G. Squires, 1971). At the same time, the $N(H)$ distribution was assumed to be Gaussian in character (typically, $N(H) > 100$) (see Fig. 1a) at each height, there is no correlation between signals at different heights, and the curvature of the fitted line can be neglected.

The ratio of the flare light to the return signal $(N_{\text{after}} + N_{\text{back-dark}})/N_{\text{signal}}$ becomes less than 0.01 for heights lower than ~50 km. Therefore, the flare light should only be estimated for mesospheric altitudes.

Summarizing, we can note that, disregarding the calibration error which, when included, leads to the underestimation of R, for typical signal accumulation time periods of 1.5–2 h, the total error $\delta R/R$ is ~2% at heights of 30–60 km, increases to 5% towards 70 km, and further increases to 10% towards 75 km until reaches ~20% towards 80 km.

Figure 1b shows the altitudinal profile of the scattering ratio, smoothed using a Gaussian filter, and the corridor of the total error $\pm\delta R$. The error corridor was chosen to be one standard deviation $\pm\delta R$, as is typically done to represent lidar data (Russell et al., 1979; Samokhvalov et al., 1987; Elnikov et al., 1988). That is because aerosol layers are not identified according to a single point of the profile, but rather according to a series of data points recorded successively. Given a normal distribution of the data points, a single point goes beyond, e.g., the upper boundary of the error corridor $\pm\delta R$ with a probablility of ~0.16, and three neighboring data points will do so with a probability as low as ~0.004. In our case, δR is the root-mean-square error of a single independent measurement point. Applying smoothing, we obtain a crude estimate of the regression line for the statistical data, i.e., the results of lidar sensing. On the other hand, the root-mean-square error of the position of the regression line, drawn through a few points, is estimated to be 2–3 times smaller than δR.

As can be seen from Fig. 1b, aerosol layers were observed on October 28, 2007, in the mesospheric region at heights of 60–80 km; they had scattering ratio maxima $R \approx 1.25$ at about 75 km and $R \approx 1.1$ at about 65 km. Weak aerosol scattering with $R \approx 1.05$ was observed in the region of the upper stratosphere. The R measurement error sharply increased above 80 km and confined sensing to below this height.

4. PHOTOPHORESIS-RELATED FORMATION MECHANISM OF AEROSOL LAYERS IN THE STRATOSPHERE AND MESOSPHERE

As was already indicated in the Introduction, the phenomenon of photophoresis for aerosol particles is well confirmed both experimentally and theoretically. Photophoresis arises when aerosol particles residing in a rarefied gas medium absorb visible and IR radiation and have temperatures other than that of the gas environment. Consider an aerosol particle with a convex shape. The force acting on a unit area at surface point s will be approximately equal to $p + p\alpha_s\Delta T_s/(4T)$, where p and T are the temperature and pressure of the gas medium; $\Delta T_s = (T_s - T)$ is the difference between the temperatures of gas and surface T_s; and α_s is the accommodation coefficient of gas molecules, which, in the framework of the model that was suggested by Maxell, is treated as the probability that a molecule will be reflected from a surface with temperature T_s diffusely (otherwise, it will be reflected specularly with the probability $1 - \alpha_s$). The force exerted by gas on the particle is written as

$$\mathbf{F}_{ph} = \frac{p}{4T}\int_S \alpha_s \Delta T_s d\mathbf{S} \tag{3}$$

and is called the photophoretic force. Here, the integration is over the entire particle surface, and the vector of the elementary area $d\mathbf{S}$ is directed along the inner normal to the surface.

When the accommodation coefficient is constant across the particle surface, a photophoretic force of the ΔT type arises. Beginning from the work of Hidy and Brock (1967), a number of theoretical works calculated this photophoretic force for the case of an ideally uniform spherical particle. The force arises in the direction coinciding with that of the incident radiation and, sometimes, in the opposite direction. This is because the light field inside the particle is distributed symmetrically relative to the direction of radiation propagation and, consequently, both the heat release inside the particle and the surface temperature are symmetrically distributed. For the upper stratosphere and mesosphere, these forces are too weak to counteract the gravitational force and to lift particles (Beresnev et al., 2003).

If the accommodation coefficient varies across the particle surface, the so-called $\Delta\alpha$-type photophoretic forces arise. In this case, the nonuniformity of the temperature distribution over the particle surface can be neglected.

In this work, the photophoretic forces were calculated for a model quasi-spherical particle. This particle has a spherical surface. One of its hemispheres has the α_1 accommodation coefficient; the other one, α_2. By integrating (3), we obtain a formula that can be used to calculate the force

$$F_{ph} = \Delta\alpha \Delta T_s S p/(4T), \tag{4}$$

where S is the particle surface area and $\Delta\alpha = (\alpha_1 - \alpha_2)/4$ is the parameters that characterize the effective dispersion of the accommodation coefficient over the particle surface. The photophoretic force will be directed along the particle symmetry axis away from the hemisphere with the larger α value towards the hemisphere with the smaller α value.

In the general case when a particle has an arbitrary shape and internal structure, the $\Delta\alpha$-type photophoretic force will be constant in magnitude and direction in the coordinate system rigidly associated with the particle body, and the force will change its direction together with the particle orientation in space if viewed in a coordinate system, which is stationary relative to the Earth's surface. If the particle orientation changes quite chaotically, the mean projections of this photophoretic forces onto the axes of the reference system stationary relative to the Earth's surface will be close to zero. It is noteworthy that the photophoretic force will not influence the mean particle speed in the vertical direction when averaged on timescales exceeding the characteristic times of chaotic changes in the direction of the photophoretic force (0.1 s and shorter). However, in the atmosphere, there are particles (Pueshel et al., 2000) which, as they move in the field of the gravitational force, may produce a torque of force, which stabilizes the particle orientation and, hence, the direction of the photophoretic force relative to the vertical axis. In this case, the mean projection of the photophoretic force onto the vertical axis is called gravito-photophoretic force. Particles influenced by a downward-directed gravito-photophoretic force undergo accelerated sedimentation. When this force acts in the opposite direction, the sedimentation is decelerated and even particle levitation may occur. This effect is associated with the particle nonuniformity, leading to the displacement of the centers, where viscous friction and photophoresis forces are applied, relative to the center of gravity.

Our quasi-spherical model of aerosol particles assumes that the center of gravity is displaced away from the center of the spherical surface, because a particle has a nonuniform density in the direction of the hemisphere, the surface of which has a larger accommodation coefficient. From an analysis of the motion of this particle in the gravitational field, it follows (Rohatschek, 1996) that there appears a stable particle orientation and gravito-photophoretic force that counteracts the gravitational force if the temperature of the particle exceeds the temperature of the surrounding gas. Random molecular disturbances of the particle orientation reduce the mean projection of the photophoretic force onto the vertical axis; i.e., they reduce the photophoretic force $F_{g\alpha} = F_{ph}L(x)$, where F_{ph} is photophoretic force (4); $L(x) = \coth(x) - 1/x$ is the Langevin function with the argument $x = qG/(kT)$, where G is the weight of the particle; k is the Boltzmann constant; and q is the displacement of the center of gravity away from the center of the sphere. Molecular disturbances of the particle orientation lead to the fact that particles with diameter D less than a certain critical diameter D_L (Cheremisin et al., 2005) equal to 1 μm in the order of magnitude cannot move in the opposite direction of the gravitational force. For particles with a near-critical size, the mean projection of the photophoretic force onto the vertical axis $F_{g\alpha} \approx 0.7F_{ph}$, and, as particles grow in size, the Langevin factor tend to unity inversely proportional to the fourth degree of the particle diameter: $L(x) \approx 1 - (D_L/D)^4$. The D_L critical diameter is inversely proportional to $q^{1/4}$; therefore, changing displacement q by a factor of 10 alters D_L by a factor of 2 only. Therefore, for particles able to levitate, the choice of specific q is of little significance. In this work, we chose $q = 0.2D$.

The temperature of the particle surface was calculated according to the condition of thermal balance under the assumption that the particle achieved the stationary thermal regime:

$$H + \Phi^V_{abs} + \Phi^{IR}_{abs} - \Phi^{IR}_{emi} = 0,$$

where H is the energy flux transferred by gas molecules to the particle surface; Φ^{IR}_{abs} and Φ^V_{abs} are the particle-absorbed fluxes of terrestrial IR radiation and visible solar radiation, respectively; and Φ^{IR}_{emi} is the particle-emitted flux of IR energy. In the free molecular regime approximation, $H = -\bar{\alpha} c_{ef} v_T (p/4kT) S\Delta T$ (Cheremisin et al., 2005), where $\bar{\alpha} = (\alpha_1 + \alpha_2)/2$ is the mean accommodation coefficient; $v_T = \sqrt{8kT/\pi m}$ is the thermal speed of molecules; m is the mean mass of gas molecules; $c_{ef} = c_V + k/2$ is the effective thermal capacity of gas per single molecule; and c_V is the thermal capacity of gas at a constant volume ($c_{ef} \approx 3k$ for diatomic molecules of the basic atmospheric gases). The radiative fluxes were calculated according to the following formulas: $\Phi^V_{abs} = (\pi D^2/2)\sigma T_B^4 \varepsilon(T_B)$; $\Phi^{IR}_{emi} = \pi D^2 \sigma T_s^4 \varepsilon(T_s)$. Here, I_V = 1.368 kW/m^2 is the solar constant, T_{Sun} = 6000K is the effective temperature of the Sun, and σ is the Stefan–Boltzmann constant. Terrestrial IR radiation was represented as the emission of a surface with effective temperature T_B. The T_B temperature was determined on the basis of the formula $\sigma T_B^4 = E^{IR}_\sigma$, where E^{IR}_σ is the flux density of terrestrial IR radiation, which was determined according to the ERBE satellite data (Barkstrom and Smith, 1986). Data on the outgoing thermal radiation were monthly averaged for specified latitudes and longitudes. The radiation coefficients $\varepsilon(T_{Sun})$, $\varepsilon(T_B)$, and $\varepsilon(T_s)$ were calculated from the formula $\varepsilon(T) = \int J(\lambda) u_\lambda(T) d\lambda \Big/ \int u_\lambda(T) d\lambda$, where $u_\lambda(T)$ is the Planck spectral distribution for the corresponding temperature; λ is the wavelength; $J(\lambda) = 4A(\lambda)/\pi D^2$ is the absorption efficiency factor; and $A(\lambda)$ is the absorption cross-section of particles. These coefficients have the meaning of the mean (or effective) relative absorption cross-sections. The absorption cross-sections for particles were calculated according to the Mie theory (Bohren and Huffman, 1986). In this work, we considered a class of particles, which absorb well both solar radiation and terrestrial IR radiation. The particle optical properties were specified with the help of the complex refractive index; it was considered to be wavelength-independent and equal to (1.95–0.66i); i.e., it corresponded to the optical characteristics of soot (Rohatschek, 1996).

Earlier, it was shown (Cheremisin et al., 2005) that, with a high level of accuracy, the relative gravito-photophoretic force F_{ga}/G is proportional to the β force parameter, which makes it possible to take into account both the density and the accommodation characteristics of particles, and is defined as

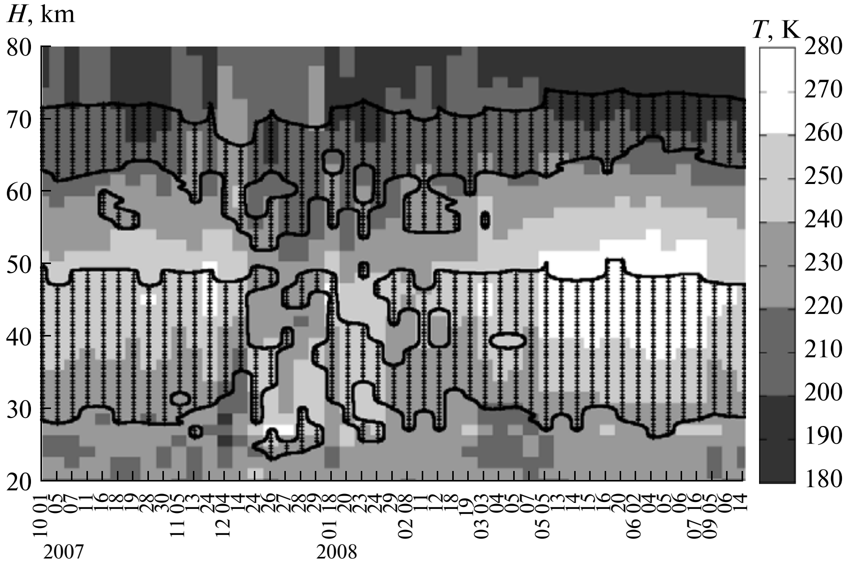

Fig. 2. Seasonal–altitudinal distribution of the atmospheric temperature according to the Aura satellite data (grayscale) for Kamchatka, the settlement of Paratunka, which is compared with calculations of the altitude regions where aerosol particles can levitate (contoured and hatched regions).

$$\beta = 2\frac{\rho_0}{\rho}\frac{\Delta\alpha}{\bar{\alpha}}, \quad (5)$$

where ρ is the density of particles and ρ_0 is some characteristic density, the value of which was chosen to be equal to the water density (1000 kg/m^3). When $\rho = \rho_0$, the force parameter $0 \leq \beta \leq 1$. The fulfillment of the $F_{g\alpha}/G \geq 1$ condition leads to the levitation of a particle, i.e., to its motion in the vertical direction opposite to the gravitational force.

Figure 2 presents calculations of the heights at which levitation of aerosol particles can occur for the days and conditions of lidar observations in Kamchatka; they are compared with the atmospheric temperatures available from the Aura satellite data. The abscissa axis indicates successive observation dates. The Aura satellite data were taken for the subsatellite point closest to the observation site in Kamchatka on the corresponding day of observations. As defined by (5), the β force parameter was chosen to be 0.035. For a quasi-spherical model of aerosol particles, when the particle density $\rho = \rho_0$, a small interhemispheric spread in the accommodation coefficients ($\alpha_1 = 0.76$ and $\alpha_2 = 0.84$) will correspond to this β value. For more loose and less dense particles, less diverging accommodation characteristics are required. The characteristic diameter of levitating particles is 1–2 μm.

As can be seen from Fig. 2, similar to soot particles, which absorb well visible and IR radiation, a characteristic feature of these particles is the existence of two altitude regions in the upper stratosphere and mesosphere, where particles can levitate under the impact of the gravito-photophoretic force. The first region is located below the stratopause at heights of 30–50 km. The second region is at heights of 60–75 km between the temperature maximum and minimum in the mesosphere. Stratospheric warming events led to a more complex pattern of levitation regions in December and January. At that time, the temperature maximum subsided to 40 km; moreover, there were two to three more local temperature maxima in the atmosphere.

As the β force parameter increases compared to $\beta = 0.035$, the two-layer levitation pattern on the whole remains unaltered. Only some minor details change, in particular, the upper boundary of the mesospheric layer levels off, attaining heights of 73–75 km. As β decreases, both layers narrow and even disappear at a certain minimal critical value of this parameter.

5. COMPARISON OF LIDAR OBSERVATIONS AND ALTITUDE REGIONS OF GRAVITO-PHOTOPHORETIC LEVITATION

Due to weather conditions, a total of 47 nighttime observations were performed in the time period from October 2007 to September 2008. With the gray level scale ranging between white and dark-gray, Fig. 3 presents the altitudinal profiles of the scattering ratio obtained for different dates of observations. The scattering ratio was calculated using Aura satellite data on the atmospheric temperature and pressure on observation days. In order to be confident that aerosol scattering, and not just a measurement error, was present, it was assumed that there were no aerosols when the scattering ratio dropped below the preset threshold $R_{\text{threshold}} = 1.05$. This region is shown in white. Moreover, each profile of the scattering ratio was confined

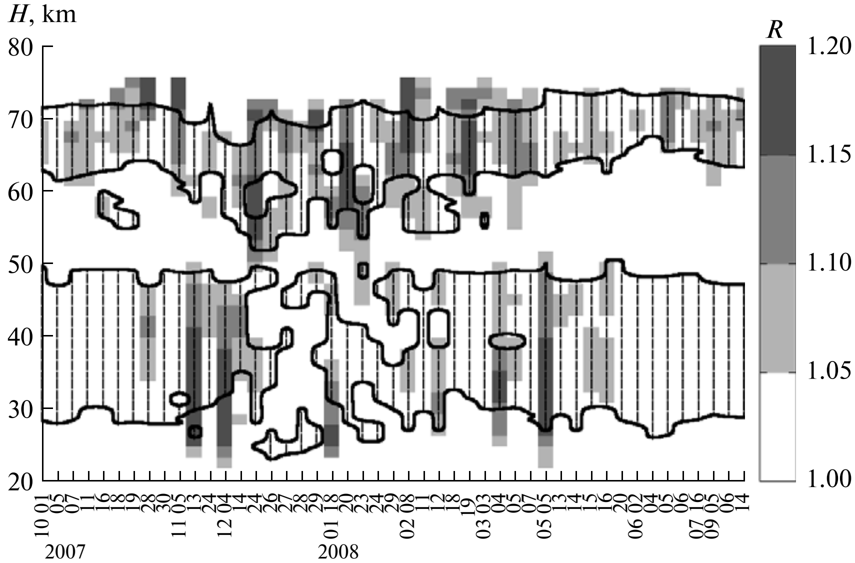

Fig. 3. Seasonal–altitudinal distribution of the *R* backscattering ratio (grayscale) according to lidar observations in Kamchatka (the settlement of Paratunka), which is compared with calculations of the altitude regions where aerosol particles can levitate (contoured and hatched regions). The calculations were based on the Aura satellite data on density and pressure.

in altitude from reliability considerations of the aerosol scattering estimate. The region above this boundary (higher than 70–75 km) is also shown in white, as is the region where no aerosol scattering is present.

An analysis of the lidar observations makes it possible to identify two periods with different features of occurrence of aerosol layers in the upper stratosphere and mesosphere. The first "warm" season lasts from May to October, and the remaining part of the year accounts for the "cold" season. Pronounced stratospheric and mesospheric layers of aerosol scattering are present during the "cold" season within the altitude intervals of 30–50 and 60–75 km. During the "warm" season, the stratospheric layer almost disappears; the scattering ratio is on the whole close to unity; and lidar signals well correspond to Rayleigh molecular scattering during this season. At the same time, in the region of the mesospheric layer, there is weak aerosol scattering.

Figure 3 also presents calculated altitude regions, where aerosol particles can levitate under the impact of gravito-photophoretic forces (these same regions are also presented in Fig. 2). The calculations used the same Aura satellite data on the pressure and temperature as was done to retrieve the profiles of the scattering ratio according to lidar measurements.

A comparison of the calculated levitation regions of aerosol particles with the seasonal–altitudinal pattern of aerosol scattering (Fig. 3) allows us to identify the following general features. The primary feature is the characteristic two-layer pattern of aerosol scattering and levitation regions as a whole. It is noteworthy that, on the whole, during the entire one-year observation period, the aerosol-scattering layers were well superimposed on the altitude regions where levitation can occur. The lidar data suggest that the lower boundary of the mesospheric aerosol scattering layer is at higher altitudes in the "warm" season as compared to the "cold" one. The mesospheric levitation region exhibits a similar regularity. In December and January, during stratospheric warming events, the stratospheric and mesospheric aerosol layers become much closer in altitude and more structured. A similar pattern is also characteristic of levitation regions.

Thus, we can conclude that the structure and seasonal changes in the aerosol scattering layers observed correspond well to the levitation regions calculated.

Data of atmospheric models are often used to calculate the molecular scattering in retrievals of the backscattering ratio from lidar returns. These models contain averaged characteristics of the atmosphere that can differ markedly from the current actual characteristics, obtained with the help of balloon sonde or satellite measurements. Figure 4 presents calculations of the levitation regions and retrievals of aerosol scattering from lidar measurements with the use of the NRLMSISE-2000 atmospheric model (Picone et al., 2002) instead of satellite data on the temperature and pressure at different heights in the atmosphere.

As can be seen from Fig. 4, the MRLMSISE-2000 model, used to calculate the gravito-photophoretic force, also gives the two-layer pattern of the altitude regions where the levitation of aerosol particles can occur. The retrievals of the scattering ratio from lidar data also reveal the presence of two layers of elevated aerosol scattering: mesospheric and stratospheric layers. This figure differs most significantly from Fig. 3 during the "cold" period of stratospheric warming

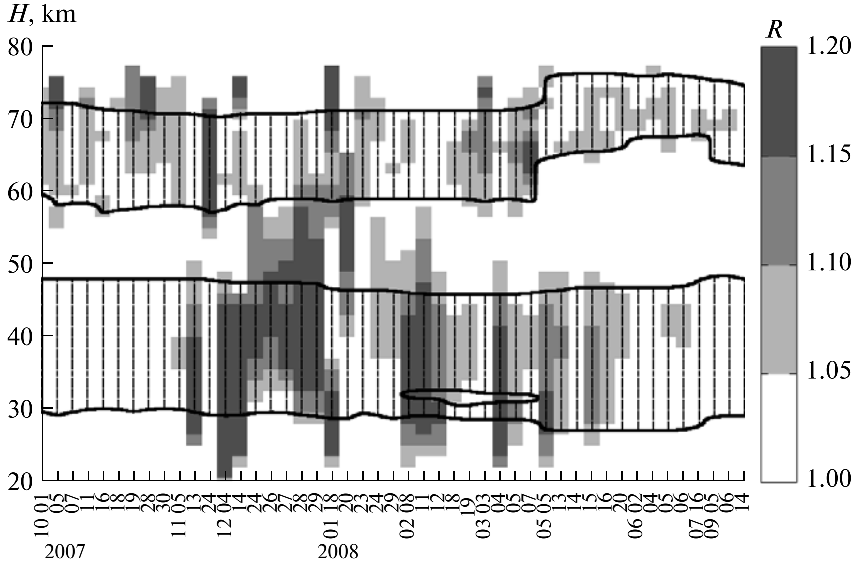

Fig. 4. Same as in Fig. 3, except that the calculations used the NRLMSISE-2000 model data on density and pressure.

events in December–January: the stratospheric and mesospheric levitation regions do not come close together and have a relatively simple structure, while the aerosol scattering layers merge into a single wide layer at heights of 30–65 km. Thus, during strong disturbances of the atmosphere, due to stratospheric warming events, the use of averaged model characteristics of the atmosphere instead of satellite estimates of the current values of these characteristics, leads to marked uncertainties both during retrievals of the backscattering ratio and during determinations of the levitation regions.

6. CONCLUSIONS

The improvement of the method and technique of lidar observations made it possible to obtain data on aerosol scattering in the upper stratosphere and mesosphere over Kamchatka (the settlement of Paratunka) at heights of 30–80 km. Observations were conducted during a year from October 2007 to September 2008 and indicated the occurrence of aerosol layers in the upper stratosphere at heights of 30–50 km and in the mesosphere at heights of 60–75 km.

We calculated the altitude regions where aerosol particles can levitate under the impact of gravito-photophoretic forces for the conditions of lidar observations over Kamchatka. The calculations used the Aura satellite data on temperature and pressure, as well as the ERBE satellite data on terrestrial IR radiation.

A comparison of experimental observations and theoretical calculations showed that the structure and seasonal variations in the observed aerosol scattering layers corresponded well to the calculated levitation regions. Taking into consideration that gravito-photophoretic forces can sustain particles at specific heights, particles can accumulate to form aerosol layers at these heights. Therefore, it can be concluded that the stratospheric and mesospheric aerosol layers detected at heights of 30–50 and 60–75 km, respectively, can be explained by the occurrence of gravito-photophoretic force, which leads to the levitation of aerosol particles at these heights.

ACKNOWLEDGMENTS

This work was supported by the Russian Foundation for Basic Research (project no. 10-05-00907-a), the Ministry of Education and Science of the Russian Federation (project no. 2.1.1/6996), the Presidium of the Russian Academy of Sciences (program no. 16), and by the Far Eastern Branch, Russian Academy of Sciences (program no. 9-II-CO-07-001).

REFERENCES

Atmosfera. Spravochnik (The Atmosphere: A Manual), Sedunov, Yu.S., Ed., Leningrad: Gidrometeoizdat, 1991.

Barkstrom, B.R. and Smith, G.L., The Earth Radiation Budget Experiment: Science and Implementation, *Rev. Geophys.*, 1986, vol. 24, no. 2, pp. 379–390.

Beresnev, S.A., Kovalev, F.D., Kochneva, L.B., Runkov, V.A., Suetin, P.E., and Cheremisin, A.A., On the Possible Photophoretic Levitation of Particles in the Stratosphere, *Opt. Atmos. Okeana*, 2003, vol. 16, no. 1, pp. 52–57.

Bohren, C., Huffman, D, *Absorption and Scattering of Light by Small Particles*, Moscow: Mir, 1986.

Bronshten, V.A., *Serebristye oblaka i ikh nablyudenie* (Noctilucent Clouds and Their Observation), Moscow: Nauka, 1984.

Butov, V.V. and Loginov, S.V., Restoration of Distribution of Ozone and Certain Aerosol Characteristics in the Stratosphere Using the Method for Sounding the Earth's Twilight Aureole from Space, *Opt. Atmos. Okeana*, 2001, vol. 14, no. 8, pp. 697–703.

Bychkov, V.V. and Marichev, V.N., Production of Water Aerosols in the Upper Stratosphere during an Anomalous Winter Absorption of Radiowaves in the Ionosphere, *Opt. Atmos. Okeana*, 2008, no. 3, pp. 248–255.

Bychkov, V.V., Marichev, V.N, Perezhogin, A.S., Shevtsov, B.M., and Shumeiko, A.V., Dynamics of Lidar Reflections in the Kamchatka Mesosphere during an Anomalous Winter Absorption of Radiowaves in the Ionosphere, *Opt. Atmos. Okeana*, 2008, no. 12, pp. 1083–1087.

Bychkov, V.V., Perezhogin, A.S., Shevtsov, B.M., Marichev, V.N., Novikov, P.V., and Cheremisin, A.A., Consideration of the Photomultiplier Pulse Aftereffect in Lidar Signals in the Kamchatka Middle Atmosphere, *Opt. Atmos. Okeana*, 2011, vol. 24, no. 2, pp. 107–113.

Cheremisin, A.A., Transfer Matrices and Solution of the Heat–Mass Transfer Problem for Aerosol Clusters in a Rarefied Gas Medium by the Monte Carlo Method, *Rus. J. Numer. Anal. Math. Modelling (RJNAMM),* 2010, vol. 25, no. 3, pp. 209–233.

Cheremisin, A.A. and Vassilyev. Y.V., Numerical Calculation Gravito-Photophoretic Movement for Aerosol Aggregates, *A. Deepak Publ.*, 2006, vol. 148, pp. 131–135.

Cheremisin, A., Granitskii, L., Myasnikov, V., and Vetchinkin, N., Improved Aerosol Scattering in the Upper Atmosphere according to Data of Ultraviolet Observations from Space, with Instrumental Smoothing Taken into Account, *Proc. SPIE*, 2000, vol. 4341, pp. 383–389.

Cheremisin, A.A., Vassilyev, Yu.V., and Kushnarenko, A.V., Photophoretic Forces for Bispherical Aerosol Particles, *Proc. SPIE*, 2002, vol. 5027, pp. 21–32.

Cheremisin, A.A., Vassilyev, Yu.V., and Horvath, H., Gravito-Photophoresis and Aerosol Stratification in the Atmosphere, *J. Aerosol. Sci.*, 2005, vol. 36, no. 11, pp. 1277–1299.

Dobber, M.R., Dirksen, R.J., Levelt, P.F., et al., Ozone Monitoring Instrument calibration, *IEEE Trans. Geosc. Rem. Sens.*, 2006, vol. 44, no. 5, pp. 1209–1238.

El'nikov, A.V., Krekov, G.M., and Marichev, V.N., Lidar Observations of the Stratospheric Aerosol Layer over Western Siberia, *Fiz. Atmos. Okeana*, 1988, vol. 24, no. 8, pp. 818–823.

Fiedler, J., Baumgarten, G., and Lübken, F.-J., NLC Observations during One Solar Cycle above ALOMAR, *J. Atmos. Sol.–Terr. Phys.*, 2009, vol. 71, pp. 424–433.

Friedrich, M. and Rapp, M., News from the Lower Ionosphere: A Review of Recent Developments, *Surv. Geophys.*, 2009a, vol. 30, pp. 525–559.

Friedrich, M., Torkar, K.M., Singer, W., Strelnikova, I., Rapp, M., and Robertson, S., Signatures of Mesospheric Particles in Ionospheric Data, *Ann. Geophys.*, 2009, vol. 27, pp. 823–829.

Giovane, F., Schnerman, D.W., and Greenberg, J.M., The Solar Occultations Technique for Remote Sensing of Particulated in the Earth's Atmosphere. 2: Skylab Results of 48 km Aerosol Layers, *J. Geophys. Res.*, 1976, vol. 81, no. 30, pp. 5383–5388.

Hervig, M.E., Gordley, L.L., Stevens, M.H., Russell, IIIJ.M., Bailey, S.M., and Baumgarten, G., Interpretation of SOFIE PMC Measurements: Cloud Identification and Derivation of Mass Density, Particle Shape, and Particle Size, *J. Atmos. Sol.–Terr. Phys.*, 2009, vol. 71, pp. 316–330.

Hidy, G.M. and Brock, J.R., Photophoresis and Descent of Particles in the Lower Atmosphere, *J. Geophys. Res.*, 1967, vol. 72, pp. 455–460.

Kent, G.S. and Wright, R.W.H., A Review of Laser Radar Measurements of Atmospheric Properties, *J. Atmos.–Terr. Phys.*, 1970, vol. 32, no. 5, pp. 917–943.

Kondrat'ev, K.Ya., Buznikov, A.A., and Pokrovskii, O.M., Determining Aerosol Vertical Profiles in the Atmosphere Based on the Spectrophotometry of the Earth's Twilight Horizon from the "Soyuz-13" Spacecraft, *Dokl. Akad. Nauk SSSR*, 1977, vol. 235, no. 1, pp. 53–56.

Krekov, G.M. and Zvenigorodskii, S.G., *Opticheskaya model' srednei atmosfery* (Optical Model of the Middle Atmosphere), Novosibirsk: Nauka, 1990.

Kuznetsov, G.I., Sitnik, G.F., Chizhov, A.F., and Shtyrkov, O.V., Certain Optical Characteristics of the Atmosphere Obtained with Meteorological Rockets MR-12 and MR-100, *Meteorol. Issled.*, 1977, no. 23, pp. 21–29.

Mezheris, R., *Lazernoe distantsionnoe zondirovanie* (Laser Remote Sensing), Moscow: Mir, 1987.

Mikirov, A.E. and Smerkalov, V.A., *Issledovanie rasseyannogo izlucheniya verkhnei atmosfery Zemli* (Studying Scattered Radiation of the Earth's Upper Atmosphere), Leningrad: Gidrometeoizdat, 1981.

Picone, J.M., Hedin, A.E., Drob, D.P., and Aikin, A.C., NRLMSISE-00 Empirical Model of the Atmosphere: Statistical Comparisons and Scientific Issues, *J. Geophys. Res.*, 2002, vol. 107, pp. 1469–1483.

Poultney, S.K., Laser Radar Studies of Upper Atmosphere Dust Layers and the Relation of Temporary Increases in the Dust to Cometary Micrometeoroid Streams, *Space Res.*, 1972, vol. 12, pp. 403–421.

Pueshel, R.F., Verma, S., Rohatschek, H., Ferry, G.V., Boiadjieva, N., Howard, S.D., and Strawa, A.W., Vertical Transport of Anthropogenic Soot Aerosol into the Middle Atmosphere, *J. Geophys. Res.*, 2000, vol. 105D, pp. 3727–3736.

Rapp, M. and Lübken, F.-J., Polar Mesosphere Summer Echoes (PMSE): Review of Observations and Current Understanding, *Atmos. Chem. Phys.*, 2004, vol. 4, pp. 2601–2633.

Rohatschek, H., Levitation of Mesospheric and Stratospheric Aerosols by Gravito-Photophoresis, *J. Aerosol Sci.*, 1996, vol. 27, no. 3, pp. 467–475.

Rössler, F., Aerosol Layers in the Atmosphere, *Space Res.*, 1972, vol. 12, pp. 423–431.

Rozenberg, G.V. and Sandomirskii, A.B., Optical Stratification of Atmospheric Aerosol, *Izv. Akad. Nauk SSSR, Fiz. Atmos. Okeana*, 1971, vol. 7, no. 7, pp. 737–749.

Rozenberg, G.V., Gorchakov, G.I., Georgievskii, Yu.S., and Lyubovtseva, Yu.S., Optical Parameters of Atmospheric Aerosol, in *Fizika atmosfery i problemy klimata*. (Physics of the Atmosphere and Climate Problems), Golitsyn, G.S., Ed., Moscow: Nauka, 1980, pp. 216–256.

Russell, P.B., Swissler, T.J., and Patrick McCormick, M., Methodology for Error Analysis Simulation of Lidar Aerosol Measurements, *Appl. Opt.*, 1979, vol. 18, no. 22, pp. 3783–3797.

Samokhvalov, I.V., Kopytin, Yu.D., Ippolitov, I.I., et al., *Lazernoe zondirovanie troposfery i podstilayushchei poverkhnosti* (Laser Sounding of the Troposphere and Underlying Surface), Zuev, V.E, Ed., Novosibirsk: Nauka, 1987.

Squires, G.L., *Practical Physics*, Cambridge: Cambridge Univ. Press, 1985. Translated under the title *Prakticheskaya fizika*, Moscow: Mir, 1971.

Vetokhin, S.S., Gulakov, I.R., and Pertsev, A.I., *Odnoelektronnye fotoprietmniki* (Single-Electron Optosensor), Moscow: Energoatomzidat, 1986.

Zeller, O., Zecha, M., Bremer, J., Latteck, R., and Singer, W., Mean Characteristics of Mesosphere Winter Echoes at Mid- and High-Latitudes, *J. Atmos. Sol.–Terr. Phys.*, 2006, vol. 68, pp. 1087–1104.